Influence of intermolecular interactions and size effect on LITH-FORC diagram in 1D spin crossover compounds

A. ROTARU*, A. GRAUR, G.-M. ROTARU[a], J. LINARES[b], Y. GARCIA[c]
Faculty of Electrical Engineering and Computer Science, "Stefan cel Mare" University, 720229, Suceava, Romania.
[a] *EMPA Materials Science and Technology, Laboratory for Protection and Physiology, Lerchenfeldstrasse 5, CH-9014 St. Gallen, Switzerland*
[b] *"Groupe d'Etude de la Matière Condensée" (GEMaC), CNRS-UMR 8635, UVSQ, 78035 Versailles Cedex, France*
[c] *Institute of Condensed Matter and Nanosciences, MOST – Inorganic Chemistry, Université Catholique de Louvain, Place L. Pasteur, 1, 1348 Louvain-la-Neuve, Belgium*

The First-order Reversal Curve (FORC) method is employed to analyze the influence of intermolecular interactions and particle size effect on Light-induced Thermal Hysteresis (LITH) behaviour of 1D spin crossover systems. We have used *atom-phonon coupling* model in order to simulate LITH-FORC diagrams with different interactions strengths and various amounts of molecules. The obtained FORC diagrams are rather different, which make this method a very powerful characterization tool. Finally, a comprehensive image of the particle size and interaction influence on the statistical parameters characterizing the LITH-FORC diagram is presented.

(Received April 19, 2012; accepted June 6, 2012)

Keywords: Molecular bistability / Spin crossover / Memory effect / FORC/ LITH

1. Introduction

Besides the interesting fundamental aspects, potential applications, such as memories, switching devices, displays and sensors [1,2] continue to draw attention to the spin crossover (SCO) phenomenon [3,4], which involves reversible spin state switching in some $3d^{4-7}$ transition metal complexes by various external perturbations such as temperature, pressure, light irradiation, magnetic or electrical field [3-6].

The bistable nature of SCO materials coupled to their sensitivity to light irradiation is of particular interest for the development of data recording media [7]. At low temperature (typically below 80 K), the system can be reversibly switched from the ground low-spin (LS) state to the metastable high-spin (HS) state using appropriate wavelengths. These phenomena are known as LIESST and Reverse-LIESST effects, respectively [8,9]. Experiments under permanent irradiation illustrate the competition between the *non-cooperative* photoexcitation and the *cooperative* thermally activated HS to LS relaxation leading to a Light-Induced Thermal Hysteresis (LITH) [10,11].

Theoretical and experimental studies in this area have focused on the origins of cooperativity, i.e. the degree of interactions among the switching molecules, resulting in an abrupt or hysteretic spin transition [12-16]. Conventional macroscopic methods, such as measurements of major hysteresis loop, only provide information about global behavior of hysteretic systems (with the shape, be symmetric or asymmetric and width extent), but they can also yield ambiguous results. Due to the various combinations of ligands nature, grain size, internal stress or elastic interactions among the SCO molecules, different systems can be characterized by the same critical temperatures and the same shape of the hysteresis loop, but with completely different behavior inside the hysteresis loop. In an attempt to remove some of the ambiguity inherent to conventional hysteresis measurements, Pike et al. [17] developed a characterization method using a type of hysteresis curve called First-Order Reversal Curve (FORC). Due to its simplicity and the wealth of information provided, FORC diagram became popular in the study of coercivity and interaction spectra in ferromagnetic nanostructured systems [17 – 24]. Moreover, FORC diagram was used successfully to understand other systems presenting hysteretic behaviour such as ferroelectric materials [25, 26] and more recently, for the first time, for SCO materials with pressure, thermal and light induced thermal hysteresis providing useful insights to cooperative effects of these magnetic systems [27-32]. The FORC diagram allows indeed a direct access to the interactions distribution of the system. In the case of ferromagnetic materials, the correlation of the FORC diagram with the intrinsic physical parameters is well understood; however, in the case of SCO materials it is still to be clarified [28, 29, 32].

We present herein a systematic theoretical investigation of the intermolecular elastic interactions as well as size effect on the LITH-FORC diagrams in the framework of *"atom-phonon coupling"* (APC) model solved in the mean field approximation. Indeed, size effects have become particularly attractive in the SCO area with potential applications in mind, and in this frame, several miniaturization studies have already been undertaken [33-36].

2. Atom-phonon coupling model

For understanding the qualitative features of the experimental FORC distributions associated with the LITH loops, we have proceeded to various simulations using the mean field approach of the APC model. The APC model which was firstly presented by Nasser et al. [37] has been further developed to explain different exotic or unusual magnetic behaviors, such as: two steps thermal spin transitions [38], the relaxation of the photo-induced metastable states and LITH curves [39-41], pressure induced re-entrance phase transitions [42,43] which has been observed experimentally in SCO molecular systems, including a 1D chain [44]. The extension of the APC model to the 2D lattice has also been recently proposed [45].

In the APC model, the SCO molecules are modeled as atoms linked by springs. Depending on the spin state of the neighboring molecules; three values of the elastic constants are taken into account: λ, when both molecules are in the LS state, ν, when both molecules are in the HS state, and μ, for the mixed spin state situation when one atom is in the LS state and its neighbor is in the HS state (see Fig. 1).

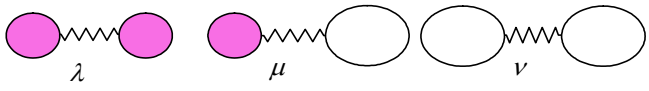

Fig. 1 Elastic constants corresponding to the spin state of the nearest neighbor pair of atoms (LS in pink and HS in white).

In the mean field approximation, two order parameters are introduced: $m=\langle\hat{\sigma}\rangle$ and $s=\left\langle\sum\hat{\sigma}_i\hat{\sigma}_j\right\rangle$, where $\hat{\sigma}$ is the Ising-like fictitious-spin associated to each molecule. The behavior of N molecules is described by:

$$\begin{cases} m=\dfrac{\mathrm{e}^{\beta J}\cdot\sinh\left(\beta\left(-\dfrac{\Delta}{2}-\dfrac{\nu-\lambda}{4K}\cdot\dfrac{\left\langle H_{phon}(K)\right\rangle_T}{N}+k_BT\dfrac{\ln r}{2}\right)\right)}{\sqrt{e^{2\beta J}\cdot\sinh^2(\beta h)+e^{-2\beta J}}} \\ s=1-\dfrac{2\cdot\mathrm{e}^{-2\beta J}}{\left(e^{\beta J}\cosh(\beta h)+\sqrt{e^{2\beta J}\cdot\sinh^2(\beta h)+e^{-2\beta J}}\right)\cdot\sqrt{e^{2\beta J}\sinh^2(\beta h)+e^{-2\beta J}}} \end{cases}, \quad (1)$$

where:

$$h=-\frac{\Delta}{2}-\frac{\nu-\lambda}{4K}\cdot\frac{\left\langle H_{phon}(K)\right\rangle_T}{N} \quad (2)$$

$$J=-\frac{\lambda-2\mu+\nu}{8K}\frac{\left\langle H_{phon}(K)\right\rangle_T}{N}, \quad (3)$$

and

$$K=\frac{\lambda+2\mu+\nu}{4}+\frac{\nu-\lambda}{2}m+\frac{\lambda-2\mu+\nu}{4}s. \quad (4)$$

$\left\langle H_{phon}(K)\right\rangle$ is the mean value of the phonon Hamiltonian, given by:

$$\left\langle H_{phon}(K)\right\rangle=\frac{\hbar\omega_M(\lambda)}{2}\cdot\sqrt{\frac{K}{\lambda}}\cdot \cdot\sum_{(i)}\left(\left|\sin\frac{i\pi}{N}\right|\cdot\coth\left(\frac{\beta\hbar\omega_M(\lambda)}{2}\cdot\sqrt{\frac{K}{\lambda}}\cdot\left|\sin\frac{i\pi}{N}\right|\right)\right), \quad (5)$$

where $i=0,\pm1,\ldots\pm\left(\frac{N}{2}-1\right),\frac{N}{2}$, $\beta=1/(k_BT)$.

We mention here, that all the detailed calculations could be found in ref. 37.

From here, we take $\hbar\omega_M(\lambda)$ as the energy unit. $\omega_M(\lambda)$ is the maximum phonon angular frequency for a periodic chain with an elastic constant λ and is given by $\omega_M(\lambda)=2\sqrt{\frac{\lambda}{m_a}}$, where m_a is the atom mass.

In this contribution we are using the same reduced parameters as in Refs 38, 39:

- Reduced temperature: $t_r=\frac{k_BT}{\hbar\omega_M(\lambda)}$;
- The dimensionless electronic excitation energy: $\delta=\frac{\Delta}{\hbar\omega_M(\lambda)}$;
- The elastic force constant ratio: $x=\frac{\nu}{\lambda}$;
- The dimensionless parameter y defined by: $\mu=\frac{\lambda+\nu}{2}+\frac{\lambda-\nu}{2}y$.

The dimensionless parameter x is a measure of the interactions intensity of the system, a small value of x implies strong interactions in the system. According to the value of the dimensionless parameter y, μ can take values closer to λ or ν. In this study we considered the case where $y=0$ which characterizes the case when the elastic constant μ takes the mean value: $\mu=(\lambda+\nu)/2$.

The relaxation process is mainly determined by the tunnel effect at low temperatures (T < 30K) and thermally activated for higher temperatures (T > 40K). Many useful studies were undertaken by Hauser, Varret and their research groups [46-49]. In order to understand properties of the cooperative relaxation, they have looked at the properties of the HS state energy barrier.

In the framework of APC model, the thermally activate cooperative relaxation can be expressed as [39]:

$$\frac{dn_{HS}}{dt} = -n_{HS}k_{\infty}\exp\left(-\frac{\frac{E_a(0)}{\hbar\omega_m(\lambda)} - \frac{\delta}{2} - \frac{<H_{phon}(K)>_T}{N}}{t_r}\right), \quad (6)$$

where: k_∞ is the high-temperature limit of the relaxation rate and E_a is activation energy of the molecule for the HS→LS relaxation.

In the presence of a continuous irradiation of the system, the equation (6) is written as follows:

$$\frac{dn_{HS}}{dt} = -n_{HS}(t)K_{HL}(t_r, n_{HS}) + I_0\sigma(1-n_{HS}(t)), \quad (7)$$

with

$$K_{HL}(t_r, n_{HS}) = k_{\infty}\exp\left(-\frac{\frac{E_a(0)}{\hbar\omega_m(\lambda)} - \frac{\delta}{2} - \frac{<H_{phon}(K)>_T}{N}}{t_r}\right) \quad (8)$$

$I_0\sigma$ is the probability per time unit for a molecule to switch from LS to HS state (I_0 is the light beam intensity and σ is the light absorption cross section).

3. FORC diagram method

Fig. 2 shows a typical example of a FORC curve, which is obtained as follows: a temperature t_{max} high enough to yield a reversible HS fraction (n_{HS}) *vs.* temperature curve is fixed. The temperature is decreased to a starting value t_a and the HS fraction is then recorded stepwise at different temperatures, t_b until t_{max}.

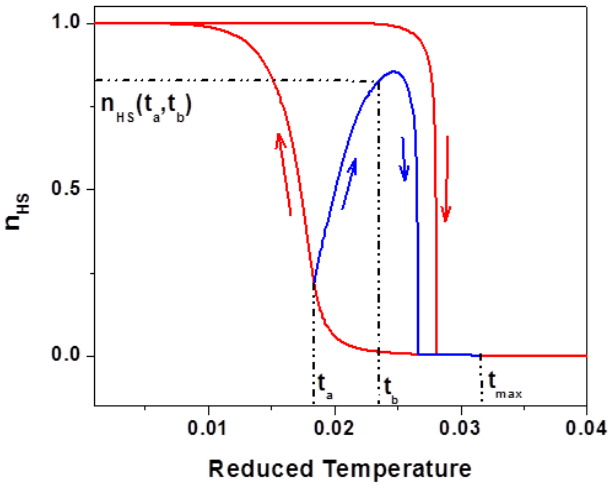

Fig. 2 Definition of FORC in the warming mode.

The FORC distributions were obtained computing the mixed second order derivative of HS fraction $n_{HS}(t_a, t_b)$, from FORC curves as a function of reversal temperature, t_a and measurement temperature, t_b using an interpolation algorithm described in Ref. 17:

$$\rho(t_a, t_b) = -\frac{1}{2}\frac{\partial^2 n_{HS}}{\partial t_a \partial t_b} \quad (9)$$

Usually a new set of coordinates (c, b) are defined with $c = (t_a - t_b)/2$ and $b = (t_a + t_b)/2$, which rotates the FORC distribution by 45°, and correspond roughly to important physical parameters such as energy gap, Δ, and Ising–like intermolecular interaction, J. Thus, the FORC diagram is a contour plot in the (c, b) plane with horizontal coercivity axis c and vertical bias axis b.

4. Results and discussions

The FORC diagram method has been already used in the characterization of the thermal kinetic and light intensity effects on LITH. However these studies have been limited to describe some particular experimental measurements [31, 32]. Herein, we would like to address some fundamental questions concerning the influence of intermolecular interactions and of the system size on the LITH-FORC diagram.

4.1 Influence of intermolecular interactions

Due to the cooperative nature of the relaxation phenomenon, the intermolecular interactions will play an important role on the LITH characteristics. We have simulated a series of FORC curves for various values of interaction intensity parameter, x and for several values of energy gap δ. The temperature rate has been kept constant in all cases. A selection of some resulting FORCs is displayed in Fig. 3. The computational parameters values are: $y = 0.0$, $r = 5$, $N = 200$, $E_a(0)/\hbar\omega_m(\lambda) = 0.8$, $k_\infty = 100$, $I_0\sigma = 0.0005\ s^{-1}$, $v = 0.001\ Ks^{-1}$.

The associated diagrams obtained from Fig 3 are reported in Fig. 4. It is clearly seen that there is a strong dependence of the FORC diagram on the magnitude of both: interactions strength and energy gap of the system. Thus, we can stress some particularities of the LITH-FORC diagrams in relation with the intermolecular interactions strength: (i) for strong intermolecular interactions (i.e. small value of x parameter) one observes a negative region (dark blue region) in good agreement with experimental observation [31]. These negative regions could be attributed to a strong mean field contribution [50]; (ii) as the interactions increase, the LITH-FORC diagram is shifting unto high coercivities

values. Here we should highlight the effect of the energy gap on the LITH-FORC distribution feature, more specifically, for high values of energy gap and high interactions strength (see in Fig. 4 the diagram obtained for δ = 0.7 and x = 0.3) a degeneration of the mean LITH-FORC diagram can be observed, giving rise to several small "islands". A similar behavior has been already noted in ferromagnetic multilayers structures [51, 52], where according to the interlayer interactions strength the magnetic domain structure is altered. However, in our case it is difficult to determine the origin of this effect; (iii) for weak interactions (i.e. high values of *x* parameter) an important reversible contribution is observed.

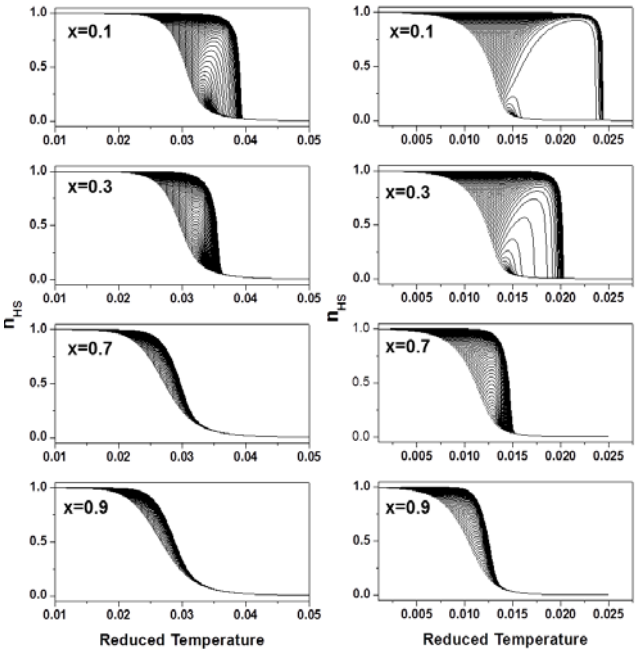

Fig. 3 Simulated FORC for different values of the interactions strength (x) for two different energy gap values: δ = 0.3 (left) and δ = 0.7 (right).

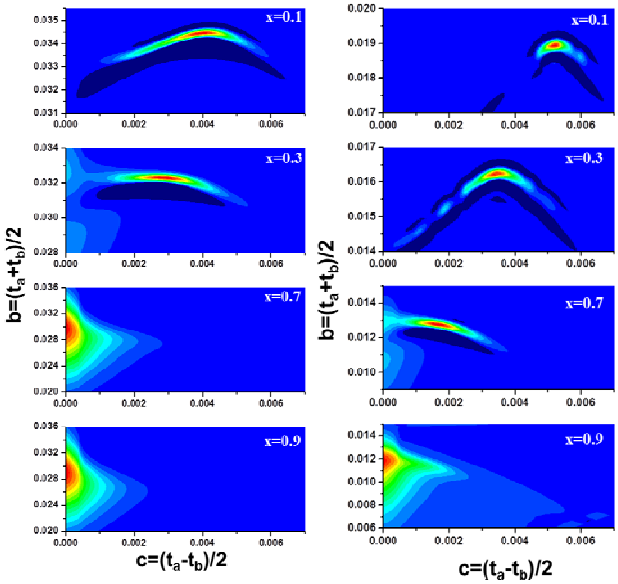

Fig. 4 Associated FORC diagrams obtained for the FORCs shown in Fig.3 for different interactions strength (x). The energy gap was: δ = 0.3 (left) and δ = 0.7 (right).

In order to compare quantitatively different FORC diagrams obtained for different values of intermolecular interactions, a statistical analysis was carried out. Hence, the distribution parameters as mean values of coercivity, $\langle c \rangle$, and bias, $\langle b \rangle$, their corresponding standard deviations, $\sigma(c)$, $\sigma(b)$ and correlation parameter r between $P(c)$ and $P(b)$ distributions were obtained [23, 27].

For a better visualization of the statistical analysis, we have plotted the interactions dependence of the main statistical parameters for different values of reduced energy gap.

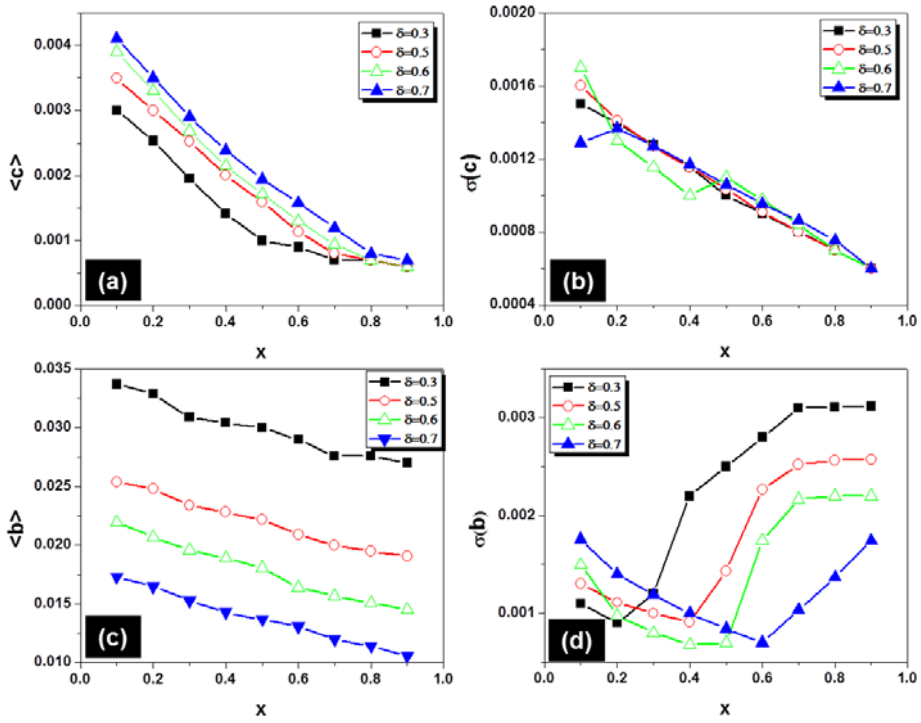

Fig. 5 Interactions strength dependece of the mean value of coercivity <c> (a), of the standard deviation of the coercivity distribution σ(c) (b), of the mean value of bias <b> (c), and of the standard deviation of the bias distribution σ(b) (d) for different values of the energy gap.

By increasing the interactions intensity (i.e. by decreasing the x parameter's value) the coercivity increases quasi-linearly. The same behaviour is observed in the dependence of the standard deviation. If for strong interactions, we can observe an increase of the coercivity with the energy gap, for weak interactions the coercivity does not depend on the energy gap. On the other hand, in almost the whole range of interactions, the standard deviation of the FORC diagrams is energy gap independent.

Regarding the bias dependency, one observes that, for a given energy gap value the mean value of the bias <b> increases as the interactions parameter x increases. This gives rise to a series of "parallel straight" lines, each line corresponding to a given energy gap value. The lowest straight line corresponds to the lower energy gap value. A more complex dependence is obtained for the standard deviation of the bias distribution $\sigma(b)$ (see Fig. 5d), which changes its monotonic variation according to the interactions strength of the system. Thus, this time, for high values of the interactions intensity, the standard deviation of the bias distribution is decreasing as the interaction decreases. After a critical value x_c of the interaction parameter, $\sigma(b)$ starts increasing as x parameter is decreasing and saturates for small values of x (e.g. $x_c = 0.6$ for $\delta = 0.7$). It is worth noting that the critical value x_c depends on the energy gap value: x_c increases as the energy gap increases.

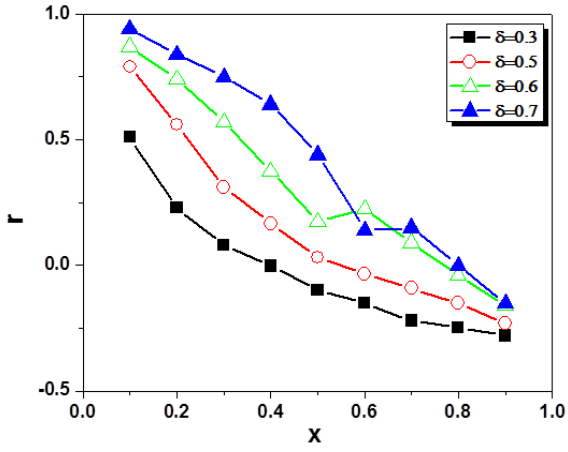

Fig. 6 Correlation parameter r as a function of the interactions strength for different values of the energy gap δ.

Another interesting result has been obtained in the variation of the correlation parameter r *vs.* x (see Fig. 6). For small values of the energy gap, the correlation parameter is decreasing exponentially with x parameter values, going from a positive correlation to a negative correlation between coercivity and bias distributions, respectively. When the energy gap value is increasing, the correlation parameter goes from an exponential dependence to a sigmoidal one, presenting an inflexion point for a critical value of the x parameter, value which depends on the energy gap δ. Finally, we note that the feature of the FORC diagrams obtained in our simulations

are similar with those obtained experimentally by Enachescu et al. [30].

4.2 Size effect

The second effect which has been studied in this work is the size effect on FORC diagrams. Concerning the photomagnetic properties of miniaturized particles, it has been observed recently on the 1D SCO coordination polymer $[Fe(NCS)_2(bpe)_2]$ (bpe = 1,2-bis(4′-pyridyl)ethane) that, the degree of conversion from the LS to the metastable HS state under irradiation (LIESST effect) is not affected by the particle size [35]. Additionally, the temperature at which the metastable state is retained, that is, the T(LIESST) value is largely unaffected by the particle size variation [35].

In order to get more information about the effect of the particle size on FORC diagram we have simulated a series of FORCs for various system dimensions (i.e. various number of molecules) and various cooperativity degrees. The computational parameters values are: $y = 0.0$, $r = 5$, $\delta = 0.6$, $E_a(0)/\hbar\omega_m(\lambda) = 0.8$, $k_\infty = 100$, $I_0\sigma = 0.0005\ s^{-1}$, $v = 0.001\ Ks^{-1}$.

The statistical analysis of the FORC diagrams obtained in our simulation is presented in Figs 7-8.

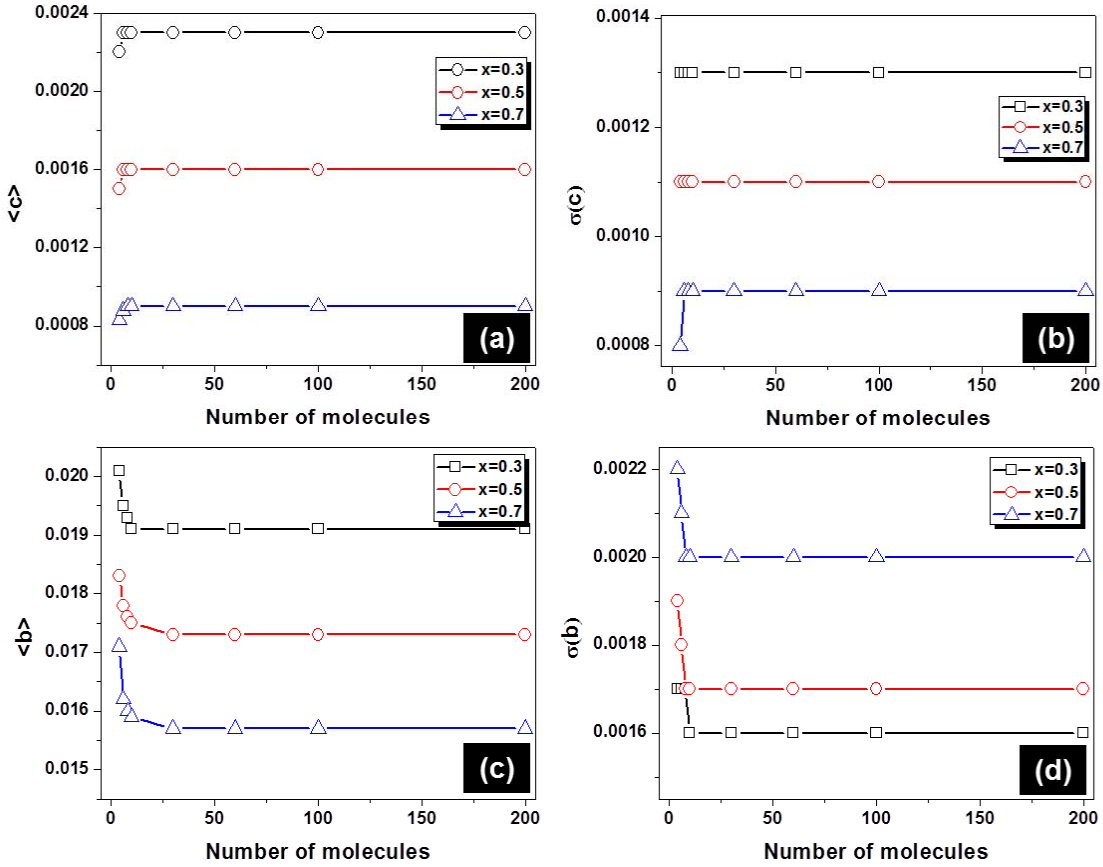

Fig. 7 Size dependence of the mean value of coercivity <c> (a), of the standard deviation of the coercivity distribution σ(c) (b), of the mean value of bias <b>, (c) and of the standard deviation of the bias distribution σ(b) (d) for different values of the interaction parameter x.

In contrast with the intermolecular interactions effect, but in good agreement with the results reported by Neville et al. [35], the size effect does not affect much the spin domain structure. Thus, as it can be seen here above the coercivity is practically unaffected by the number of molecules.

However, we can see a weak size dependence of the bias, both the mean value and the standard deviation of the bias distribution are decreasing as the number of molecules is increasing, but it rapidly saturates.

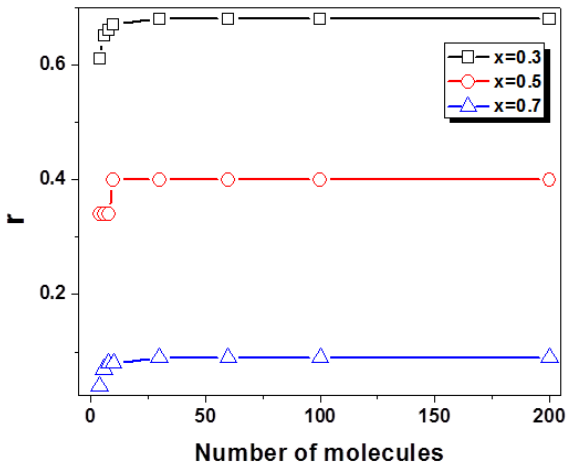

Fig. 8 Size dependence of the correlation parameter for different values of the interaction parameter.

A similar behavior is observed in the correlation parameter dependence: bellow a critical size of the system the correlation parameter is decreasing as the number of molecules decreases. We also note that the kinetic effects, which make possible the existence of a FORC distribution even in the absence of any parameter distribution, play an important role on FORC diagram.

5. Conclusions

We have used 1D atom-phonon coupling model to investigate the influence of the intermolecular interactions and of the system size on the LITH-FORC diagram in 1D spin crossover compounds. By varying progressively the cooperativity and the size of the SCO system we have been able to obtain the dependence of the statistical parameters of the FORC diagram with the interaction parameter and with the number of molecules from the system, respectively. This way we were able to give a global image on how the FORC diagram feature is modified under the influence of these parameters. An experimental study of the intermolecular interactions influence on Light-induced Thermal Hysteresis, by using FORC diagram method, will be the topic of a future investigation.

Acknowledgements

This work was partially supported by the project PRiDE, Contract no. POSDRU/89/1.5/S/57083, project co-funded from European Social Fund through Sectorial Operational Program Human Resources 2007-2013, and the Fonds National de la Recherche Scientifique (FNRS) (FRFC 2.4508.08, 2.4.537.12, IISN 4.4507.10).

References

[1] Y. Garcia, V. Ksenofontov, and P. Gütlich, Hyperfine Interact. **139/140**, 543 (2002).
[2] J. Linares, E. Codjovi, and Y. Garcia, Sensors **12**, 4479 (2012).
[3] Spin-Crossover in Transition Metal Compounds, edited by P. Gütlich and H. Goodwin, Topics in Current Chemistry, Vols. 233–325 (Springer-Verlag, Berlin, 2004).
[4] A. Bousseksou, G. Molnar, L. Salmon, W. Nicolazzi, Chem. Soc. Rev. **40**, 3313 (2011).
[5] A. Rotaru, I. Guralsky, I. A. Gural'skiy, G. Molnár, L. Salmon, P. Demont, and A. Bousseksou, Chem Commun., **48** (2012) 4163.
[6] Y. Garcia, F. Robert, A. D. Naik, G. Zhou, B. Tinant, K. Robeyns, S. Michotte, and L. Piraux, J. Am. Chem. Soc. **133**, 15850 (2011).
[7] P. Gutlich, A. Hauser, and H. Spiering, Angew. Chem., Inter. Ed., **33**, 2024 (1994).
[8] S. Decurtins, P. Gutlich, C. P. Kohler, H. Spiering, A. Hauser, Chem. Phys. Lett., **105**, 1 (1984).
[9] A. Hauser, Chem. Phys. Lett., **124**, 543 (1986).
[10] A. Desaix, O. Roubeau, J. Jeftic, J. G. Haasnoot, K. Boukheddaden, E. Codjovi, J. Linares, M. Nogues, F. Varret, Eur. Phys. J. B, **6**, 183 (1998).
[11] J. F. Letard, P. Guionneau, L. Rabardel, J. A. K. Howard, A. E. Goeta, D. Chasseau, O. Kahn, Inorg. Chem., **37**, 4432 (1998).
[12] J. F. Létard, P. Guionneau, L. Rabardel, J. A. K. Howard, A. E. Goeta, D. Chasseau, O. Kahn, Inorg. Chem. **37**, 4432 (1998).
[13] J. F. Letard, P. Guionneau, L. Goux-Capes, Spin Crossover in Transition Metal Compounds III, **235**, 221 (2004).
[14] J. F. Letard, P. Guionneau, O. Nguyen, J. S. Costa, S. Marcen, G. Chastanet, M. Marchivie, L. Goux-Capes, Chem.–Eur. J., **11**, 4582 (2005).
[15] F. Varret, K. Boukheddaden, J. Jeftic, O. Roubeau, Molec. Cryst. Liquid Cryst., **335**, 1273 (1999).
[16] C. Enachescu, L. Stoleriu, A. Stancu, A. Hauser, Phys. Rev. B, **82**, 104114 (2010).
[17] C. R. Pike, A. P. Roberts, and K. L. Verosub, J. Appl. Phys. **85**, 6660 (1999).
[18] C. Pike, A. Fernandez, J. Appl. Phys., **85**, 6668 (1999).
[19] L. Spinu, A. Stancu, C. Radu, F. Li, J. B. Wiley, IEEE Trans. Magn. **40**, 2116 (2004).
[20] D. Cimpoesu, L. Spinu, A. Stancu, IEEE Trans. Magn. **42**, 3165 (2006).
[21] F. Beron, L. Clime, M. Ciureanu, D. Menard, R. W. Cochrane, A. Yelon, J. Appl. Phys. **101**, 09J107 (2007).
[22] J. H. Yin, H. W. Zhang, F. X. Hu, B. G. Shen, L. Q. Pan, J. Appl. Phys., **106**, 103901 (2009).
[23] A. Rotaru, J.-H. Lim, D. Lenormand, A. Diaconu, J.B. Wiley, P. Postolache, A. Stancu, L. Spinu, Phys. Rev. B, **84**, 134431 (2011).

[24] A. Stancu, B. Negulescu, R. Tanasa, L. Stoleriu, Optoelectron. Adv. Mater. – Rapid Comm. **4,** 361 (2010)
[25] A. Stancu, D. Ricinschi, L. Mitoseriu, P. Postolache, M. Okuyama, Appl. Phys. Lett. **83**, 3767 (2003).
[26] O. Ovchinnikov, S. Jesse, S. Guo, K. Seal, P. Bintachitt, I. Fujii, S. Trolier-McKinstry, S. V. Kalinin, Appl. Phys. Lett. **96**, 112906 (2010).
[27] R. Tanasa, C. Enachescu, A. Stancu, J. Linares, E. Codjovi, F. Varret, J. Haasnoot, Phys. Rev. B **71**, 014431 (2005).
[28] M. M. Dîrtu, C. Neuhausen, A. D. Naik, A. Rotaru, L. Spinu, Y. Garcia, Inorg. Chem. **49**, 5723 (2010).
[29] B. Weber, W. Bauer, T. Pfaffeneder, M. M. Dîrtu, A. D. Naik, A. Rotaru, and Y. Garcia, Eur. J. Inorg. Chem., 3193 (2011).
[30] A. Rotaru, J. Linares, F. Varret, E. Codjovi, A. Slimani, R. Tanasa, C. Enachescu, A. Stancu, J. Haasnoot, Phys. Rev. B, **83** (2011) 224107.
[31] C. Enachescu, R. Tanasa, A. Stancu, F. Varret, J. Linares, E. Codjovi, Phys. Rev. B **72**, 054413 (2005).
[32] C. Enachescu, R. Tanasa, A. Stancu, G. Chastanet, J. F. Letard, J. Linares, F. Varret, J. Appl. Phys., **99**, 08J504 (2006).
[33] A. D. Naik, B. Tinant, K. Muffler, J. A. Wolny, V. Schünemann, Y. Garcia, J. Solid State Chem., **182**, 1365 (2009).
[34] A. D. Naik, L. Stappers, J. Snauwaert, J. Fransaer, Y. Garcia, Small **6**, 2842 (2010).
[35] S. M. Neville, C. Etrillard, S. Asthana, J. F. Letard, Eur. J. Inorg. Chem., 282 (2010).
[36] A. Rotaru, F. Varret, A. Gindulescu, J. Linares, A. Stancu, J. Létard, T. Forestier, C. Etrillard, Eur. Phys. J. B, **84**, 439 (2011).
[37] J. A. Nasser, Eur. Phys. J. B, **21**, 3 (2001).
[38] J. A. Nasser, K. Boukheddaden, J. Linares, Eur. Phys. J. B, **39**, 219 (2004).
[39] A. Rotaru, J. Linares, J. Optoelectron. Adv. Mater. **9**, 2724 (2007).
[40] A. Gindulescu, A. Rotaru, J. Linares, M. Dimian, J. Nasser, J. Appl. Phys., **107**, 09A959 (2010).
[41] A. Gîndulescu, A. Rotaru, J. Linares, M. Dimian, J. Nasser, Polyhedron, **30**, 3186 (2011).
[42] A. Rotaru, J. Linares, E. Codjovi, J. Nasser, A. Stancu, J. Appl. Phys. **103**, 07B908 (2008).
[43] A. Rotaru, J. Linares, S. Mordelet, A. Stancu, J. Nasser, J. Appl. Phys. **106**, 043507 (2009).
[44] Y. Garcia, V. Ksenofontov, G. Levchenko, P. Gütlich, J. Mater. Chem. **10**, 2274 (2000).
[45] J. A. Nasser, S. Topçu, L. Chassagne, M. Wakim, B. Bennali, J. Linares, Y. Alayli, Eur. Phys. J. B **83**, 115 (2011).
[46] A. Hauser, J. Chem. Phys., **94**, 2741 (1991).
[47] A. Hauser, Chem. Phys. Lett., **192**, 65 (1992).
[48] K. Boukheddaden, I. Shteto, B. Hoo, F. Varret, Phys. Rev. B, **62**, 14796 (2000).
[49] C. Enachescu, J. Linares, F. Varret, K. Boukheddaden, E. Codjovi, S. G. Salunke, R. Mukherjee, Inorg. Chem. **43**, 4880 (2004).
[50] A. Stancu, C. Pike, L. Stoleriu, P. Postolache, D. Cimpoesu, J. Appl. Phys., **93**, 6620 (2003).
[51] J. E. Davies, O. Hellwig, E. E. Fullerton, K. Liu, Phys. Rev. B, **77**, 014421 (2008).
[52] N. Siadou, M. Androutsopoulos, I. Panagiotopoulos, L. Stoleriu, A. Stancu, T. Bakas, V. Alexandrakis, J. Magn. Magn. Mater., **323**, 1671 (2011).

*Corresponding author: rotaru@eed.usv.ro